NACA

RESEARCH MEMORANDUM

LOW-SPEED LATERAL-CONTROL CHARACTERISTICS OF AN UNSWEPT

WING WITH HEXAGONAL AIRFOIL SECTIONS AND ASPECT RATIO 2.5

EQUIPPED WITH SPOILERS AND WITH SHARP- AND
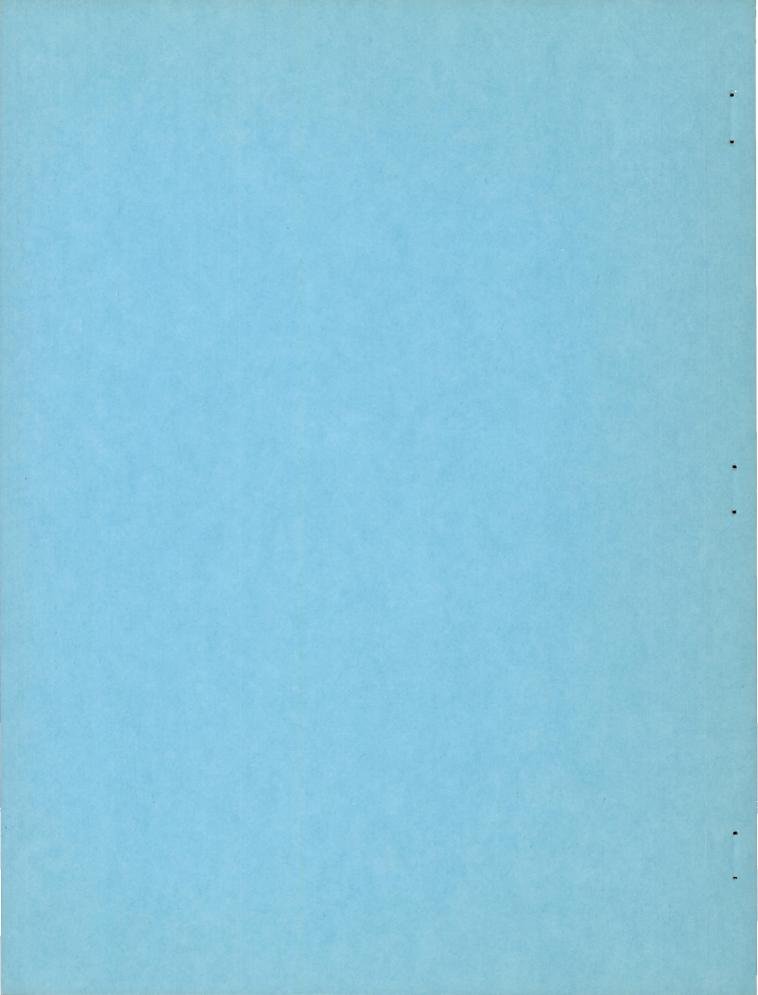
THICKENED-TRAILING-EDGE FLAP-TYPE AILERONS

AT A REYNOLDS NUMBER OF 7.6×10^6

By James E. Fitzpatrick and Robert L. Woods

Langley Aeronautical Laboratory
Langley Field, Va.

NATIONAL ADVISORY COMMITTEE
FOR AERONAUTICS
WASHINGTON
April 29, 1952

NATIONAL ADVISORY COMMITTEE FOR AERONAUTICS

———————

RESEARCH MEMORANDUM

———————

LOW-SPEED LATERAL-CONTROL CHARACTERISTICS OF AN UNSWEPT

WING WITH HEXAGONAL AIRFOIL SECTIONS AND ASPECT RATIO 2.5

EQUIPPED WITH SPOILERS AND WITH SHARP- AND

THICKENED-TRAILING-EDGE FLAP-TYPE AILERONS

AT A REYNOLDS NUMBER OF 7.6×10^6

By James E. Fitzpatrick and Robert L. Woods

SUMMARY

The lateral-control characteristics of two spans of spoiler and flap-type ailerons on an unswept wing with an aspect ratio of 2.5 and hexagonal airfoil sections are presented. The tests were conducted at a Reynolds number of 7.6×10^6 and a Mach number of 0.15. Measurements of rolling moments, yawing moments, aileron hinge moments, normal forces, and balance-chamber pressures were made for various configurations of the wing with sharp- and thickened-trailing-edge ailerons, and droop-nose and plain flaps in combination with a fuselage.

In the low-lift range, the spoilers (which projected 0.06 chord) produced rolling moments equivalent to 6° of total aileron deflection for the unflapped wing and 12° for the wing with droop-nose flap deflected. The rolling moments due to the spoiler and flap-type ailerons were reduced at angles of attack above 7° and 12°, respectively, for the unflapped configurations. The lift range through which the ailerons and spoilers remained effective was extended by deflecting the droop-nose flap.

The rolling moments due to the flap-type aileron were increased by about 30 percent and those due to the spoilers by approximately 100 percent when the span was increased from 40 to 75 percent of the semispan.

The aileron with trailing-edge-thickness ratio of 0.25 had a slightly higher value of aileron effectiveness through a small deflection range

than any other degree of trailing-edge thickness tested. At high deflections, however, the aileron with trailing-edge-thickness ratio of 1.00 was the most effective. The hinge-moment parameters became more negative with an increase in trailing-edge thickness. Calculations showed that the amount of balance chord required for complete balance in a steady roll in the low-lift range increased from 60 percent of the aileron chord for the sharp-trailing-edge aileron to 90 percent of the aileron chord for the aileron with trailing-edge-thickness ratio of 1.00.

Calculations indicate that the hinge-moment parameters in a steady roll would be smaller than those for the static condition when the droop-nose flap is not deflected.

Values of pressure-fluctuation amplitude and frequency at 10 percent of the aileron chord behind the aileron hinge line, which could be associated with buffeting, were attained at the angle of attack of initial stall. The average value of pressure fluctuation was independent of aileron deflection.

INTRODUCTION

In order to minimize drag at supersonic speeds, thin wings of low aspect ratio and relatively sharp leading edges have been proposed. A tapered wing of this type with an aspect ratio of 2.5 and thin hexagonal airfoil sections was investigated at low speed in the Langley 19-foot pressure tunnel. The results of the lateral-control investigation of the wing equipped with 0.75-semispan and 0.40-semispan flap-type and spoiler ailerons are the subject of the present paper.

The lateral-control characteristics were determined for the ailerons with several combinations of fuselage, droop-nose flap, and trailing-edge flaps. Inasmuch as the results of references 1 and 2 have indicated that improvements can be made in the rolling effectiveness of flap-type ailerons at transonic and supersonic speeds by thickening the trailing edges, the lateral-control characteristics of the 0.40-semispan aileron were also investigated on the wing with the trailing edge modified to three different thicknesses. In addition, the tests included measurements of the instantaneous pressure differential between the upper and lower surfaces at four spanwise stations.

SYMBOLS AND COEFFICIENTS

The data are referred to the wind axes with the origin at 25 percent of the mean aerodynamic chord. Symbols and nondimensional coefficients used are defined as follows:

b wing span, feet

b_s spoiler span perpendicular to plane of symmetry, feet

C_D drag coefficient $(Drag/qS)$

C_L lift coefficient $(Lift/qS)$

C_l rolling-moment coefficient $(Rolling\ moment/qSb)$

C_m pitching-moment coefficient $(Pitching\ moment/qS\bar{c})$

C_n yawing-moment coefficient $(Yawing\ moment/qSb)$

C_{h_a} aileron hinge-moment coefficient $\left(Hinge\ moment/2M_aq\right)$

C_{h_α} rate of change of C_{h_a} with α at $\delta_a = 0$

C_{h_δ} rate of change of C_{h_a} with δ_a at $\delta_a = 0$

$C_{h_\delta}{}'$ rate of change of C_{h_a} with δ_a when wing is in a steady roll

C_{l_p} rolling-moment coefficient due to rolling

C_{l_δ} rate of change of C_l with δ_a at $\delta_a = 0$

C_{N_a} aileron normal-force coefficient $\left(Normal\ force/qS_a\right)$

c local wing chord parallel to plane of symmetry, feet

$\bar{c}$ mean aerodynamic chord $\left(\dfrac{2}{S}\displaystyle\int_0^{b/2} c^2 dy\right)$

c_a aileron chord aft of hinge line and perpendicular thereto, feet

c_b aileron balance chord forward of hinge line, feet

c_{l_α} section lift-curve slope

K balance-chamber pressure conversion factor
$$\left(\frac{\text{Pressure difference across seal}}{\text{Pressure difference across vents}}\right)$$

M_a moment area of aileron aft of hinge line, taken about hinge axis, cubic feet

ΔP magnitude of resultant pressure fluctuation (difference between pressures on upper and lower surfaces), pounds per square foot

P_R converted balance-chamber pressure coefficient
$$\left(\frac{\text{Pressure below seal - Pressure above seal}}{Kq}\right)$$

P_{R_α} rate of change of P_R with α at $\delta_a = 0$

P_{R_δ} rate of change of P_R with δ_a at $\delta_a = 0$

p rolling angular velocity, radians per second

q dynamic pressure, pounds per square foot $\left(\rho V^2 / 2\right)$

S wing area, square feet

S_a aileron area aft of hinge line, square feet

t ratio of trailing-edge thickness to aileron thickness at hinge line

V free-stream velocity, feet per second

α angle of attack of root-chord line, degrees

$(\Delta\alpha)_p$ effective change in angle of attack caused by rolling velocity, degrees

δ_a aileron deflection measured in plane perpendicular to hinge
          line, positive when deflected down, degrees

δ_{a_t} sum of equal up and down aileron deflections, degrees

δ_f trailing-edge-flap deflection, degrees. (The 0.75-semispan
          and 0.35-semispan flap-type ailerons are referred to as
          flaps when both of a pair are deflected downward together.)

δ_n droop-nose-flap deflection, degrees

$\dfrac{\Delta\alpha}{\Delta\delta}$ equivalent change in angle of attack per degree flap deflection
          (two-dimensional data)

θ trailing-edge angle, degrees

ρ density of air, slugs per cubic foot

MODEL AND APPARATUS

     The details of the wing and fuselage are shown in figure 1. The
model was constructed of solid steel, painted and polished to a smooth
finish. The wing had an aspect ratio of 2.5, a taper ratio of 0.625,
and neither dihedral nor twist. The symmetrical airfoil section was
hexagonal with leading- and trailing-edge angles of 11.42°. Between
the 30- and 70-percent-chord lines the surfaces were parallel and the
wing had a thickness of 6 percent chord. The fuselage used for some
of the tests was of circular cross section and fineness ratio 8 to 1.
The wing root-chord line was on the center line of the fuselage.

     Details of the lateral-control devices are shown in figure 2. The
chord of the flap-type aileron was a constant percentage of the wing
chord (0.25c). The aileron extended from 0.20b/2 to 0.95b/2 on the left
wing and was divided at the 0.55b/2 station so that the outboard portion
could be deflected alone or in combination with the inboard portion. In
various parts of the investigation the inboard portion and both portions
were deflected 50° in combination with corresponding portions on the
right wing to simulate high-lift flaps. The trailing edge of the wing
was modified to 0.25, 0.50, and 1.00 of the wing maximum thickness for
some of the tests of the 0.40b/2 flap-type aileron. The leading edge
of the flap-type aileron was of circular-arc contour with the center
at the hinge line and was provided with a flexible seal (fig. 2). The
balance chamber was provided with orifices for measuring pressures
above and below the seal. The aileron was attached to the wing by means

of four strain-gage beams (two on each portion). The strain gages indicated electrically the aileron hinge moments and the component of the aileron force normal to the aileron-chord line. In addition, the magnitude and frequency of pressure fluctuations over the aileron were measured by means of four miniature inductance-type pressure cells installed in the sharp-trailing-edge aileron at a distance of 10 percent of the aileron chord behind the hinge line and at the spanwise positions shown in figure 1. The measurements were transmitted electrically to a recording galvanometer.

The spoilers (0.40b/2 and 0.75b/2) were mounted normal to the wing surface and projected 0.06 chord (see fig. 2). Dimensions of the 0.75b leading-edge droop-nose flap are shown in figure 1.

A two-support system was used to mount the wing alone or the wing-fuselage combination in the tunnel. A photograph of the model mounted in the tunnel is shown as figure 3.

TESTS AND CORRECTIONS

The tests were conducted in the 19-foot pressure tunnel with the air compressed to 33 pounds per square inch. The Reynolds and Mach numbers of the tests were 7.6×10^6 and 0.15, respectively.

The lateral-control characteristics of the flap-type and spoiler ailerons were determined by measuring the forces and moments through a range of angle of attack from $-4°$ through the stall with the flap-type ailerons set at various deflections. Aileron hinge moments, normal forces, and balance-chamber pressures were also measured. The 0.75b/2 sharp-trailing-edge aileron was tested both with and without the fuselage. The 0.40b/2 and 0.75b/2 sharp-trailing-edge ailerons were tested with the wing leading-edge droop-nose flap deflected 30° and the fuselage on. The 0.40b/2 aileron was tested in conjunction with the 0.30b flap, with and without the deflected droop-nose flap. Both spans of spoilers were tested with the fuselage on, with and without the deflected droop-nose flap, and with and without the 0.75b flap. The test configurations are listed in table I.

The lift and pitching-moment coefficients have been corrected for support-strut tare and interference as determined by tare tests with an image support system. The angles of attack have been corrected for air-stream misalinement as determined during the tare tests. The jet-boundary corrections to the angle of attack and drag were calculated by

the method of reference 3. Jet-boundary corrections to the rolling and yawing moments were found to be negligible. Slight rolling and yawing moments were found to exist at zero deflection due to the small air-stream misalinement across the tunnel. Corrections have been applied for these effects.

A calibration of the balance chambers indicated leakage through the seal; the pressure differences measured across the seal were only 0.80 and 0.56 of the pressure differences across the vents for the sharp and blunt ailerons, respectively. The factor was smaller for the blunt ailerons than for the sharp aileron because smaller vent openings were used with the blunt ailerons (see fig. 2). The same seal was used for all aileron configurations. Using the two conversion factors K, the measured pressure differences across the seal were converted to pressure differences across the vents which approximate balance-compartment pressure differences with a perfect seal. This approximation neglects the effects of the leakage on the vent pressures.

RESULTS AND DISCUSSION

Lateral-Control Characteristics

Spoilers.- The characteristics of the plain wing (fig. 4(a)) are indicative of the type of flow associated with unswept wings that have sharp leading edges and low aspect ratio. The rolling-moment coefficients due to the 0.40b/2 spoiler obtained in the low angle-of-attack range were about 0.01, and an increase in spoiler span to 0.75b/2 doubled this value. At angles of attack above 4°, however, the rolling moments decreased, and above 8° the longer span showed no appreciable advantage over the shorter. At angles of attack close to 7°, separation occurred near the wing leading edge (fig. 5) and the loading shifted toward the tips (reference 4). These changes in the flow are probably responsible for the abrupt reduction of spoiler rolling moments and the rearward shift in center of pressure. Because of the separated flow conditions that existed, an increase in spoiler projection would probably have little effect on the rolling moments in the high angle-of-attack range. In the low angle-of-attack range the spoilers produced small, favorable yawing moments.

At a Mach number of 1.9 (reference 5) the spoilers produced rolling-moment coefficients of about half the value presented herein. The 0.75b/2 spoiler at a Mach number of 1.9 (reference 5) produced yawing-moment coefficients which were favorable and of greater magnitude than those of the present investigation.

By deflecting the 0.75b droop-nose flap 30°, the rolling moments
due to each spoiler were increased and the angle-of-attack range for
which the spoiler remained effective was extended considerably (fig. 4(b)).
The deflected droop-nose flap changed the flow over the wing so as to
delay leading-edge separation (fig. 5). The delay of separation by the
droop-nose flap enabled the rolling-moment coefficient due to the spoiler
to increase with lift coefficient. The yawing-moment coefficients became
adverse for this configuration with the 0.75b/2 spoiler (fig. 4(b)).

With the 0.75b flap deflected 50° in combination with the deflected
droop-nose flap, the rolling moments due to the spoiler were increased
in the angle-of-attack range up to the stall (fig. 4(c)). The rolling
moments obtained with this configuration were greater than those of
either of the other two configurations. With the 0.75b flap deflected,
the yawing moments became adverse at an angle of attack lower than that
with the flap neutral. The yawing moments produced by the 0.75b/2
spoiler were more adverse than those of the 0.40b/2 spoiler (fig. 4(c)).
With the 0.75b flap deflected, the adverse yawing moment reached about
0.0225 as compared with 0.0075 for the configuration with droop-nose
flap alone (figs. 4(c) and 4(b)). At high lift coefficients in a roll,
the yawing moments would tend to become even more adverse.

Flap-type ailerons.- The aerodynamic forces and moments produced
by the deflected ailerons for the various configurations are presented
in figures 6 to 16. The aileron effectiveness C_{l_δ} was obtained from
cross plots of these data and is presented in figure 17. The effective-
ness of the 0.40b/2 aileron on the plain wing for each trailing-edge-
thickness ratio is presented in figure 17(a). For all degrees of
trailing-edge thickness, the control effectiveness was gradually reduced
throughout the lift range and a large reduction occurred near maximum
lift. The reduction in aileron effectiveness due to an increase in
trailing-edge thickness was only about 10 percent at low angles of
attack. References 1 and 2 show that an increase in rolling effective-
ness with increase in trailing-edge thickness is obtained at transonic
and supersonic speeds.

The aileron effectiveness parameter C_{l_δ} for the 0.40b/2 aileron
was calculated according to the method of reference 6. The values of
section lift-curve slope and of flap effectiveness $\Delta\alpha/\Delta\delta$ for the sharp-
trailing-edge aileron were obtained from the experimental data of
reference 7. Values of $\Delta\alpha/\Delta\delta$ and section lift-curve slope for the
thickened-trailing-edge aileron configurations were obtained by cor-
recting the values of the sharp-trailing-edge aileron for differences
in trailing-edge angle according to figure 19 of reference 8. Values
for $\left(C_{l_\delta}\right)_{calc}$ were obtained by calculating the values of C_{l_δ} for

t = 0 at given values of θ. The following are the calculated and experimental values of C_{l_δ} for the various degrees of bluntness:

t	θ (deg)	$\dfrac{\Delta\alpha}{\Delta\delta}$	c_{l_α}	$\left(C_{l_\delta}\right)_{calc}$	$\left(C_{l_\delta}\right)_{exp}$
0	13.7	0.402	0.096	0.00133	0.00140
.25	10.3	.415	.097	.00139	.00145
.50	6.9	.428	.099	.00146	.00139
1.00	0	.450	.101	.00157	.00135

Of course, this comparison does not account for the effects of finite trailing-edge thickness but it shows that trailing-edge-angle concepts cannot be used to predict effects of trailing-edge thickness. In the present investigation, the data indicate that after a certain degree of trailing-edge thickness was reached, the aileron effectiveness was reduced. Other effects, such as might be caused by flow around the base, might counteract the effect of a decreased trailing-edge angle.

The 0.40b/2 aileron on the wing with the high-lift devices showed the same general trend of effectiveness through the lift range as it did on the plain wing. Extending the span of the aileron 0.35b/2 inboard increased the effectiveness by about 30 percent in the low-lift range (figs. 17(a) and 17(b)). The calculated and experimental values of C_{l_δ} for the wing with the 0.75b/2 aileron were 0.00213 and 0.00205, respectively. The slight increase in C_{l_δ} due to the addition of a fuselage (fig. 17(b)) might mean that the fuselage acted as an end plate to increase the effectiveness of the inboard aileron. The data of references 9 and 10 indicate that at transonic and supersonic speeds the value of C_{l_δ} for the plain wing and fuselage decreased until at a Mach number of 1.9 it reached about half the value obtained at a Mach number of 0.15. This was true for both aileron spans (fig. 18).

Deflecting the partial-span flap reduced C_{l_δ} in the low-lift range (fig. 17(c)). Deflecting the droop-nose flap extended the lift range in which the aileron remained effective (fig. 17(d)); this effect was due to the postponement of separation around the sharp leading edge until higher angles of attack were reached. Increasing the aileron span resulted in an increase in effectiveness which was about the same whether or not the droop-nose flap was deflected (fig. 17).

The rolling-moment and yawing-moment coefficients produced by a total aileron deflection of 30° (15° equal and opposite) and, in some cases, 50° are presented in figures 19 and 20. Figure 19(a) shows the effect of various degrees of trailing-edge thickness. These results are quite different from the results shown by the C_{l_δ} curves of figure 17(a). The difference is a result of the nonlinearity of the curves for C_l plotted against δ. For the aileron with $t = 0.25$, the slope C_{l_δ} through zero deflection is higher than that for the aileron with $t = 1.0$, but the slope decreases at higher deflections. With the full-blunt aileron ($t = 1.0$), C_{l_δ} has a lower value through zero deflection but it is more nearly constant at higher deflections.

For the other configurations, the trends shown by the rolling-moment coefficients for a total aileron deflection of 30° are the same as those shown previously by the variations of C_{l_δ}.

The yawing moments produced by the deflected aileron tended to become more adverse as the lift increased up to the stall (figs. 6 to 16 and fig. 20). For the configurations without the deflected droop-nose flap, most of the adverse yaw was contributed by the downward-deflected aileron. This effect of the downward-deflected aileron is attributed to the difference in induced drag of the two wings. The downward-deflected aileron increased both the lift and the induced drag of its wing.

Comparison of spoilers and flap-type ailerons.- The rolling moments produced by the spoilers (which projected a distance of 0.06c) are compared with the rolling moments for several total aileron deflections in figure 21. On the unflapped wing (fig. 21(a)), the rolling moment due to the spoiler is seen to be equivalent to that for a total aileron deflection of 6°. Increasing the span of the spoiler to 0.75b/2 increases the rolling moment to that obtained with a total aileron deflection of 10° (fig. 21(b)). At a Mach number of 1.9 (references 5 and 10), the effectiveness of the 0.75b/2 spoiler was found to be equivalent to the same total aileron deflection as that found in the present investigation. Deflecting the droop-nose flap 30° makes the spoiler as effective as a total aileron deflection of 11° or 12° (figs. 21(c) and 21(d)). A similar comparison of spoilers and ailerons may be made in terms of flying qualities. The rolling effectiveness $\frac{pb}{2V}$ for the plain wing was calculated from the equation

$$\frac{pb}{2V} = -\frac{C_l}{C_{l_p}}$$

A value of -0.22 for C_{l_p} was interpolated from the theoretical curves

given in reference 6. The value of $\frac{pb}{2V}$ for the 0.40b/2 spoiler varied

from 0.043 at zero lift to 0.009 at maximum lift ($\alpha = 12^\circ$), whereas the
value for a total deflection of 30° of the 0.40b/2 flap-type aileron
varied from 0.181 at zero lift to 0.151 at maximum lift. For the 0.75b/2
aileron, the values were from 0.1 to 0.014 for the spoiler and from 0.30
to 0.24 for a total flap-type-aileron deflection of 30°.

A comparison of the yawing moments produced by oppositely deflected
ailerons with those produced by spoilers for the configurations shown
in figure 21 are presented in figure 22.

The foregoing comparisons of spoiler and aileron effectiveness must
be restricted to the low-speed range because of the following factors:

1. At higher speeds the aileron effectiveness is greatly reduced
by wing twist (reference 11). The effectiveness of a spoiler is not
reduced as much because the twisting moments due to a spoiler are of
lesser magnitude for a given rolling moment.

2. The rigid-wing spoiler effectiveness increases with speed in the
subsonic range (reference 12).

3. The higher control-force characteristics of ailerons are partially
accounted for by power-booster systems.

4. In the moderate to high-lift range the yawing moment due to the
deflected control is more adverse for ailerons than for spoilers (fig. 22),
which would reduce the superiority of the aileron over the spoiler.

Aileron Hinge-Moment Characteristics

Blunt unbalanced ailerons on the plain wing.- The hinge-moment
parameters C_{h_δ} and C_{h_α} are presented in figures 23 to 25. The

effects of seal leakage on these parameters have been neglected. With
increasing trailing-edge thickness the hinge-moment parameters increased
negatively (fig. 25). As shown in reference 8, a decrease in trailing-
edge angle also results in more-negative values of the hinge-moment
parameters. The effects of trailing-edge thickness and trailing-edge
angle were similar except that the degree of unbalance was not so great
with the thickened trailing-edge as would be expected for the same
reduction in trailing-edge angle on a sharp aileron (reference 8). The
difference is no doubt due to the change in pressure distribution brought

about by the flow around the blunt end. At angles of attack beyond the
stall, the trailing-edge thickness had little effect on the hinge-
moment parameters.

Sharp unbalanced ailerons with high-lift devices.- The negative
value of C_{h_δ} was increased by the addition of the fuselage to the wing
with the 0.75b/2 aileron, whereas the value of C_{h_α} was essentially
unchanged (figs. 23(b) and 24(b)). These effects are associated pri-
marily with the load changes over the inboard portion of the aileron
due to wing-fuselage interference. A similar effect was noted when the
aileron span was increased with the fuselage on (figs. 23(e) and 24(d)).
In the moderate angle-of-attack range, however, both parameters increased
negatively with α.

Deflecting the 0.35b flap 50° added a negative increment or an
unbalancing moment to the outboard aileron. Deflecting the droop-nose
flap 30° had little effect on C_{h_δ} but considerably reduced the neg-
ative value of C_{h_α} and extended the angle-of-attack range for reason-
able values of both parameters (figs. 23(d) and 24(c)).

The effect of several amounts of internal balance on the hinge-
moment parameter C_{h_δ} was calculated for the steady rolling condition.
The effect of a steady roll proportional to total aileron deflection
may be approximated by the following equation from reference 8 $\left(\delta_{a_t}\right.$
in the present paper has the same definition as $\Delta\delta_a$ in reference 8$\left.\right)$:

$$C_{h_\delta}{}' = C_{h_\delta} + \frac{2(\Delta\alpha)_p}{\delta_{a_t}} C_{h_\alpha}$$

The values of $2(\Delta\alpha)_p\big/\delta_{a_t}$ were estimated from the data given in
reference 8 to be $-173C_{l_\delta}$ for the 0.75b/2 aileron and $-242.2C_{l_\delta}$
for the 0.40b/2 aileron.

The effect of a sealed internal balance on the hinge-moment
characteristics was taken into account approximately by means of the
following relations:

$$\left(C_{h_\alpha}\right)_{bal} = C_{h_\alpha} + \frac{1}{2} P_{R_\alpha}\left(\frac{c_b}{c_a}\right)^2$$

and

$$\left(C_{h_\delta}\right)_{bal} = C_{h_\delta} + \frac{1}{2} P_{R_\delta}\left(\frac{c_b}{c_a}\right)^2$$

where the subscript bal refers to the aileron with an internal nose balance, and c_b/c_a is the balance-chord ratio. The measured hinge moments are assumed to be for an aileron with a perfect seal; thus the effects of the seal leakage on the hinge moments were neglected.

The values presented beyond the stall should be viewed with caution. The value of C_{l_p} used in determining $\frac{2(\Delta\alpha)_p}{\delta_{a_t}}$ was assumed constant at -0.22, whereas in reality it would tend toward zero at the stall. The positive values of C_{h_δ}' beyond the stall are therefore somewhat too high. The trends presented, however, are considered indicative of the effect of balance. The results of these calculations are presented in figure 26. A comparison of figure 23(a) with 26(a) shows that rolling had a slight balancing effect, reducing C_{h_δ} by about 0.001 in each case. The amount of balance chord required for balance in the low and moderate lift range increased from about $0.6c_a$ for the sharp aileron to about $0.9c_a$ for the ailerons with t = 0.50 and t = 1.0.

The addition of a fuselage tended to balance the 0.75b/2 aileron for $c_b/c_a = 0$, but did not affect the balance chord required for complete balance (fig. 26(b)). Rolling had little effect on the aileron hinge-moment parameter C_{h_δ} when the droop-nose flap was deflected. The aileron balance chord required for balance was about 0.65 at $0.85C_{L_{max}}$. With the droop-nose flap deflected, an increase in aileron span increased the degree of unbalance with no balance chord but did not change the $0.65c_a$ balance chord required for balance at $0.85C_{L_{max}}$ (fig. 26(c)). The values presented are more nearly applicable in the low-speed high-lift range, since increasing the Mach number has a tendency to increase the degree of unbalance (references 8 and 13). An estimate made from the results of reference 8 indicates that to balance the aileron at a Mach number of 0.8 would probably require a balance-chord ratio about 0.1 higher than the ratios presented in figure 26.

Measurement of Pressure Fluctuation

A sample of the records obtained with the recording galvanometer of the pressure fluctuation over the aileron is shown in figure 27. Certain amplitudes may be considered average (see, for example, that designated $\Delta P/q$ in fig. 27) and they are plotted against angle of attack for several spanwise locations and two deflections of the 0.40b/2 aileron in figure 28. The curves of figure 28 indicate that the amplitudes of the pressure fluctuations increase with angle of attack and, beyond the stall, attain values approximately equal to the dynamic pressure.

Figure 28 may give an indication of the stall-warning characteristics of an airplane equipped with this type of wing. According to the correlation of pressure pulsations with flight buffeting (reference 14), when the amplitude of the fluctuations reaches 0.15q, buffeting will be encountered. This value is reached at an angle of attack of about 6.5° in all cases (fig. 28). This is also the angle of attack at which the pitching moment breaks in a stable direction (fig. 4) and the separated flow spreads rearward over the wing (fig. 5).

CONCLUSIONS

The results of the lateral-control investigation of two spans of spoiler and flap-type ailerons on an unswept wing with an aspect ratio of 2.5 and thin hexagonal airfoil sections lead to the following conclusions:

1. In the low-lift range, the spoilers (which projected a distance of 0.06c) produced rolling moments equivalent to 6° of total aileron deflection for the wing without flaps and 12° for the wing with droop-nose flap deflected.

2. The rolling moments due to the spoiler and flap-type ailerons were reduced at angles of attack above 7° and 12°, respectively, for the unflapped configuration. Deflecting the droop-nose flap extended the lift range in which the ailerons and spoilers remained effective.

3. The rolling moments due to the aileron were increased by about 30 percent and that of the spoiler by approximately 100 percent, by extending the spans from 40 to 75 percent of the semispan.

4. An increase in trailing-edge-thickness ratio from 0 to 1.0 resulted in only a 10-percent change in aileron effectiveness.

5. The amount of balance chord required for balance in a steady roll has been calculated to increase from $0.6c_a$ for the sharp-trailing-edge aileron to $0.9c_a$ for the thickened-trailing-edge aileron.

6. A steady roll did not reduce the magnitude of the aileron hinge-moment parameters with the droop-nose flap deflected as it did when the droop-nose flap was not deflected.

7. The amplitude of average pressure fluctuation at $0.10c_a$ behind the hinge line increased with angle of attack and attained values approximately equal to the dynamic pressure. The amplitude of the fluctuations at which flight buffeting may be obtained ($0.15q$) were attained at the angle of attack of initial stall.

Langley Aeronautical Laboratory
    National Advisory Committee for Aeronautics
        Langley Field, Va.

REFERENCES

1. Fields, E. M., and Strass, H. Kurt: Free-Flight Measurements at
       Mach Numbers from 0.7 to 1.6 of Some Effects of Airfoil-Thickness
       Distribution and Trailing-Edge Angle on Aileron Rolling Effective-
       ness and Drag for Wings with 0° and 45° Sweepback. NACA RM L51G27,
       1951.

2. Goin, Kennith L.: Investigation at a Mach Number of 1.9 and a
       Reynolds Number of 2.2×10^6 of Several Flap-Type Lateral-Control
       Devices on a Wing Having 42.7° Sweepback of the Leading Edge.
       NACA RM L9A18a, 1949.
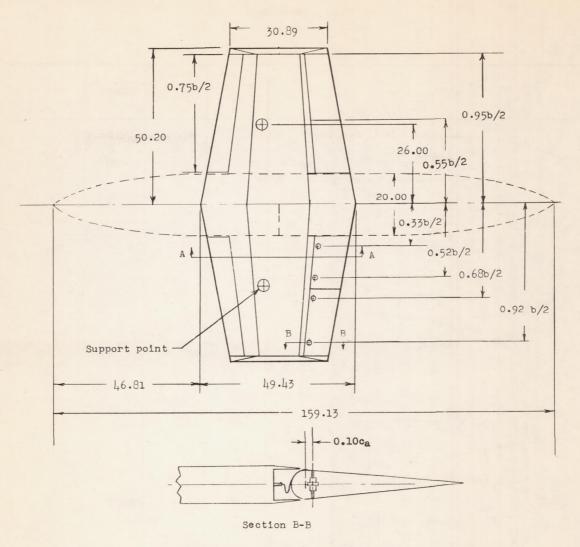
3. Silverstein, Abe, and White, James A.: Wind-Tunnel Interference with
       Particular Reference to Off-Center Positions of the Wing and to the
       Downwash at the Tail. NACA Rep. 547, 1936.

4. Winter, H.: Flow Phenomena on Plates and Airfoils of Short Span.
       NACA TM 798, 1936.

5. Conner, D. William, and Mitchell, Meade H., Jr.: Effects of Spoiler
       on Airfoil Pressure Distribution and Effects of Size and Location
       of Spoilers on the Aerodynamic Characteristics of a Tapered Unswept
       Wing of Aspect Ratio 2.5 at a Mach Number of 1.90. NACA RM L50L20,
       1951.

6. DeYoung, John: Theoretical Antisymmetric Span Loading for Wings of
       Arbitrary Plan Form at Subsonic Speeds. NACA TN 2140, 1950.

7. Underwood, William J., and Nuber, Robert J.: Two-Dimensional Wind-
       Tunnel Investigation at High Reynolds Numbers of Two Symmetrical
       Circular-Arc Airfoil Sections with High-Lift Devices. NACA RM L6K22,
       1947.

8. Langley Research Staff (Compiled by Thomas A. Toll): Summary of
       Lateral-Control Research. NACA Rep. 868, 1947. (Formerly
       NACA TN 1245.)

9. Vogler, Raymond D., Lockwood, Vernard E., and Turner, Thomas R.: An
       Investigation at Transonic Speeds of the Effects of Control Chord
       and Span on the Control Characteristics of a Tapered Wedge-Type
       Wing of Aspect Ratio 2.5. Transonic-Bump Method. NACA RM L51G03,
       1951.

10. Mitchell, Meade H., Jr.: Effects of Varying the Size and Location
        of Trailing-Edge Flap-Type Controls on the Aerodynamic Characteristics
        of an Unswept Wing at a Mach Number of 1.9. NACA RM L50F08, 1950.

11. Cooney, T. V., and Wollner, Bertram C.: A Comparison of Flight
     Measurements with Calculations of the Loss in Rolling Effective-
     ness Due to Wing Twist. NACA RM L8F07, 1948.

12. Rogallo, Francis M., Lowry, John G., and Fishel, Jack.: Lateral-
     Control Devices Suitable for Use with Full-Span Flaps. Jour. Aero.
     Sci., vol. 17, no. 10, Oct. 1950.

13. Thompson, Robert F.: Investigation of a 42.7° Sweptback Wing Model
     to Determine the Effects of Trailing-Edge Thickness on the Aileron
     Hinge-Moment and Flutter Characteristics at Transonic Speeds.
     NACA RM L50J06, 1950.

14. Humphreys, Milton D.: Pressure Pulsations on Rigid Airfoils at
     Transonic Speeds. NACA RM L51I12, 1951.

TABLE I

TEST CONFIGURATIONS

Configuration	Aileron span, percent b/2	Spoiler span, percent b/2	Figure	Presented
	— —	0.40 .75	4(a) 4(a)	c_L, c_D, c_m, c_n, c_l
$\delta_n = 30°$	— —	.40 .75	4(b) 4(b)	- do -
$\delta_f = 50°(0.75b \text{ flap})$ $\delta_n = 30°$	— —	.40 .75	4(c) 4(c)	- do -
$t = 0$	0.40	—	6	P_R, c_{N_a}, c_l, c_n, c_{h_a}
$t = 0.25$	.40	—	7	- do -
$t = 0.50$	.40	—	8	- do -
$t = 1.00$	.40	—	9	- do -
$t = 0$	.75	—	10	- do -
	.75 .40	— —	11 12	- do - - do -
$\delta_f = 50°(0.35b \text{ flap})$	.40	—	13	- do -
$\delta_f = 50°(0.35b \text{ flap})$ $\delta_n = 30°$	.40	—	14	- do -
$\delta_n = 30°$	.40 .75	— —	15 16	- do - - do -

NACA

30.89

0.75b/2

50.20

0.95b/2

26.00

0.55b/2

20.00

0.33b/2

0.52b/2

0.68b/2

0.92 b/2

A   A

B   B

Support point

46.81   49.43

159.13

0.10c$_a$

Section B-B

Location of pressure cells

0.30c   0.40c   0.30c

0.06c

0.15c   0.25c

NACA

Section A-A
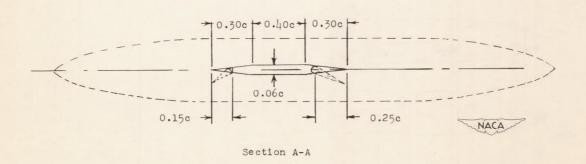
Figure 1.- Plan and sections of model. Aspect ratio 2.5; wing area
    28 sq ft; taper ratio 0.625. All dimensions are in inches unless
        otherwise noted.

(a) Sharp aileron.

(b) Blunt aileron.

(c) Spoilers.
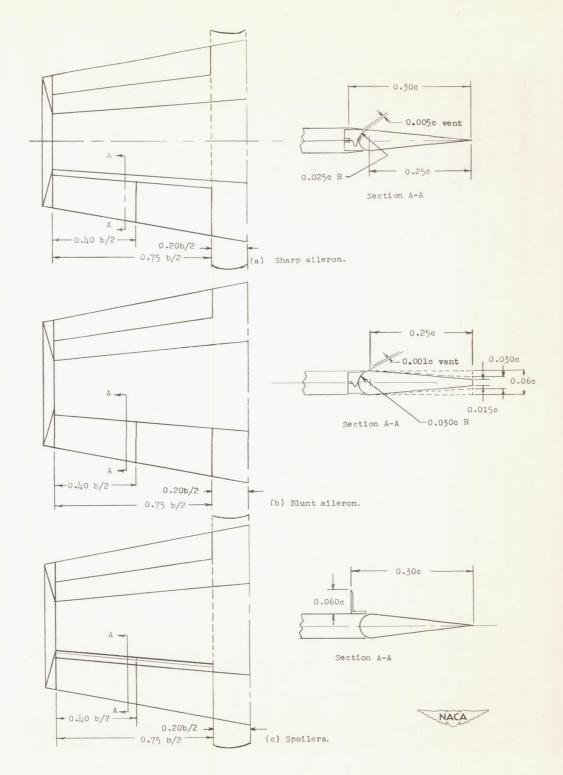
Figure 2.- Diagrams of lateral-control devices.
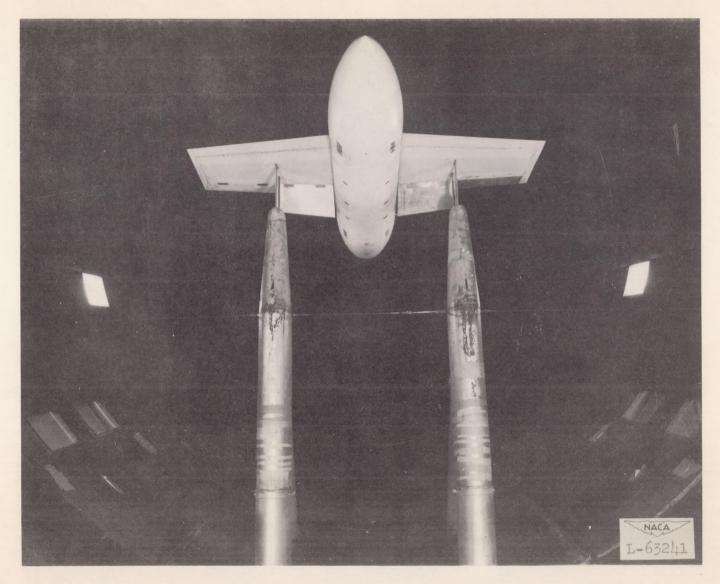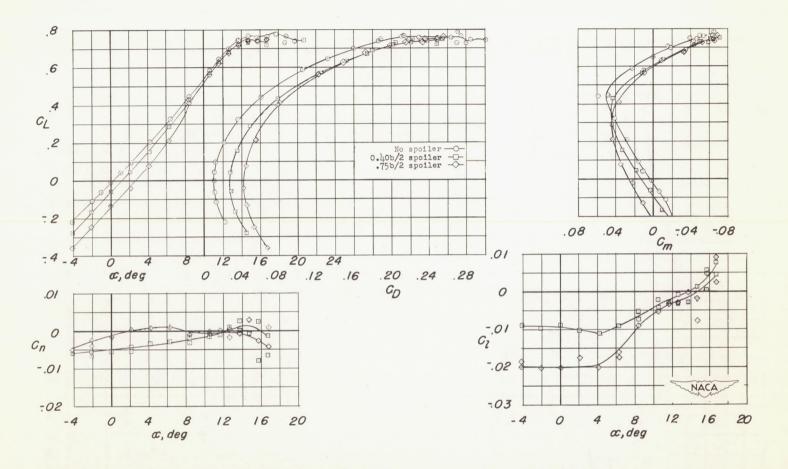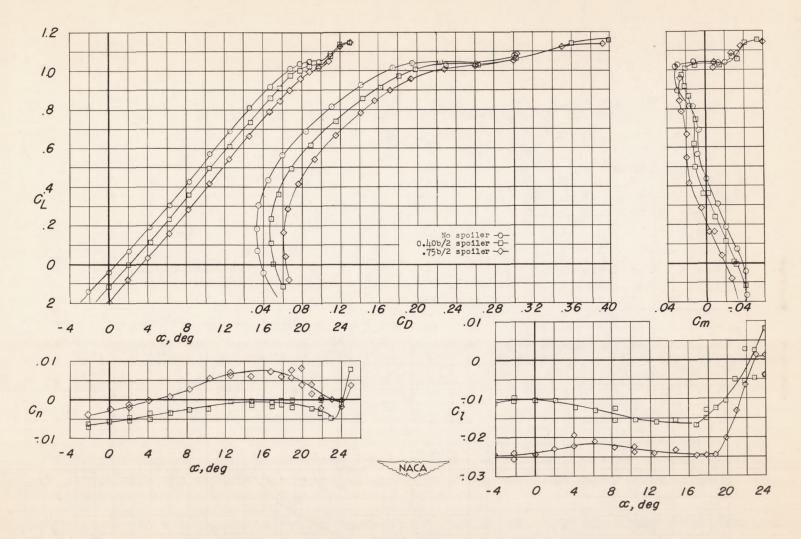
Figure 3.- Model mounted with fuselage on two-support system in
Langley 19-foot pressure tunnel.
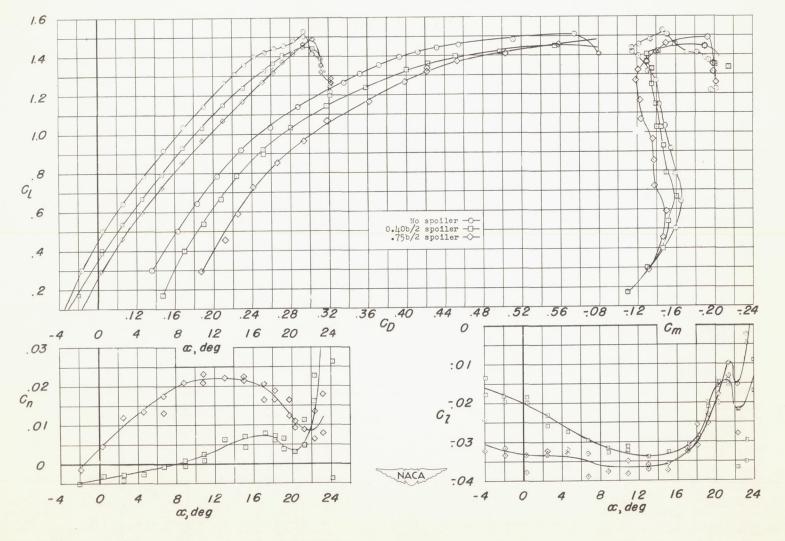
(a) Wing-fuselage combination; $\delta_n = 0^\circ$, $\delta_f = 0^\circ$.

Figure 4.- Lateral-control characteristics of the model with spoilers
that project a distance of 0.06c.

(b) Wing-fuselage combination; $\delta_n = 30^\circ$, $\delta_f = 0^\circ$.

Figure 4.- Continued.

(c) Wing-fuselage combination; $\delta_n = 30°$, $\delta_f = 50°$ (0.75b flap).

Figure 4.- Concluded.

Direction
of flow

Stalled flow

(a) Plain wing.

(b) Fuselage on; $\delta_n = 30°$.

(c) Fuselage on; $\delta_n = 30°$, $\delta_f = 50°$ (0.35b flap).
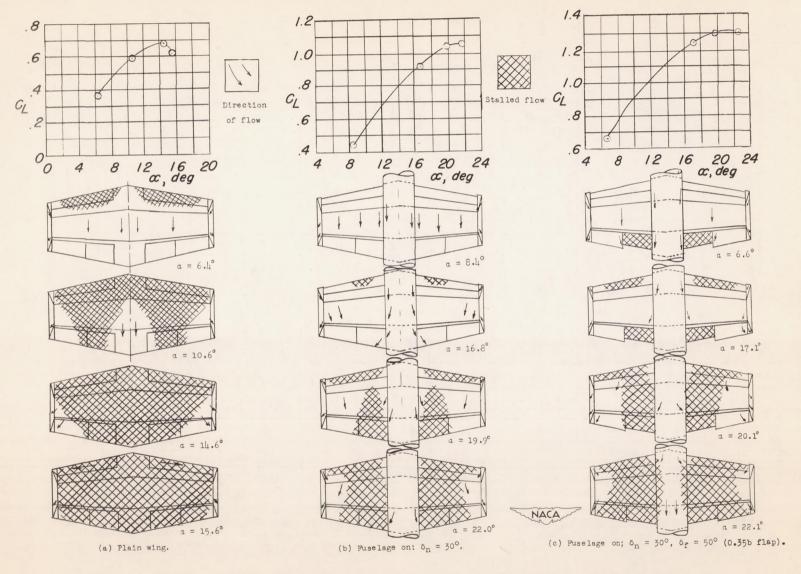
Figure 5.- Stalling patterns of the hexagonal wing model with and without
a fuselage and deflected flaps.
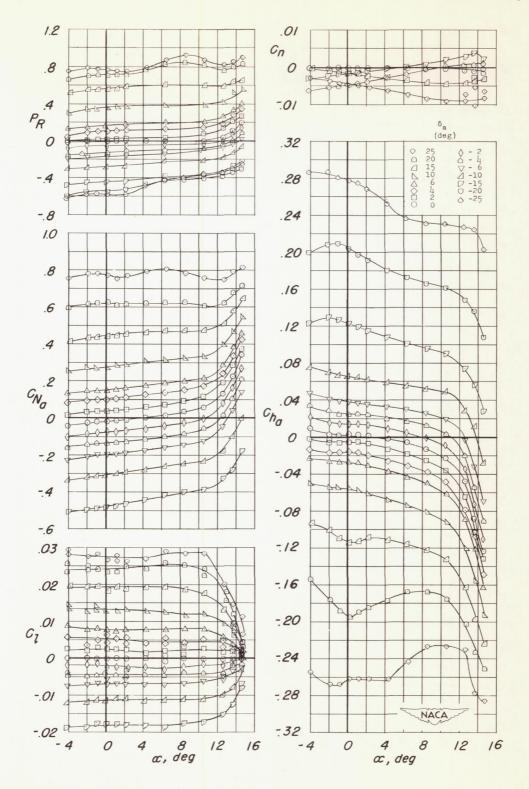
Figure 6.- Variation of P_R, C_{N_a}, C_l, C_n, and C_{h_a} with α; plain wing, $0.40b/2$ aileron, $t = 0$, $0.005c$ vent, $\delta_f = 0$, $\delta_n = 0$.
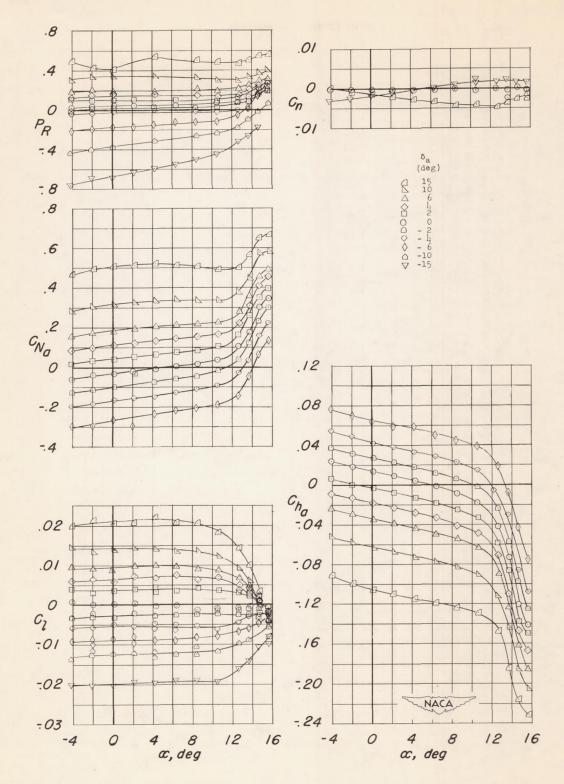
Figure 7.- Variation of P_R, C_{N_a}, C_l, C_n, and C_{h_a} with α; plain wing, 0.40b/2 aileron, t = 0.25, 0.001c vent, $\delta_f = 0$, $\delta_n = 0$.
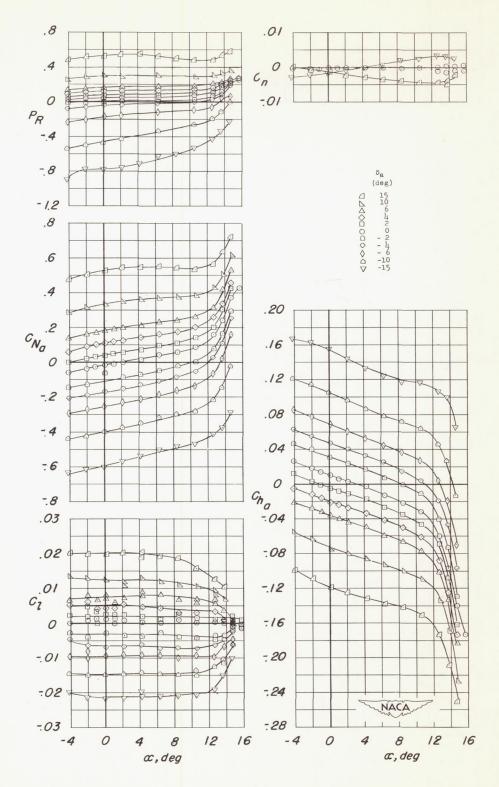
Figure 8.- Variation of P_R, C_{N_a}, C_l, C_n, and C_{h_a} with α; plain wing, 0.40b/2 aileron, $t = 0.50$, 0.001c vent, $\delta_f = 0$, $\delta_n = 0$.
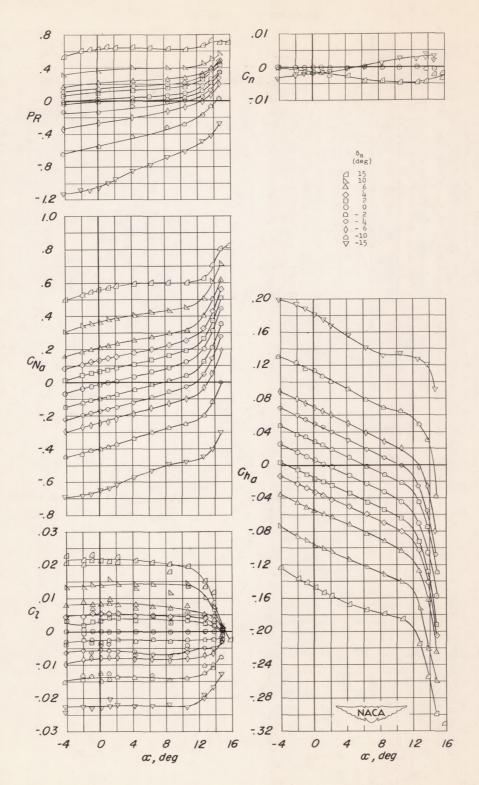
Figure 9.- Variation of P_R, C_{N_a}, C_l, C_n, and C_{h_a} with α; plain wing, 0.40b/2 aileron, t = 1.00, 0.001c vent; $\delta_f = 0$, $\delta_n = 0$.
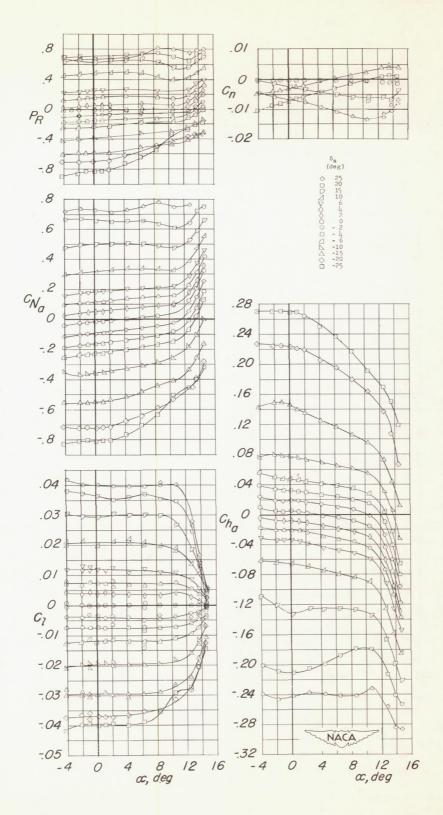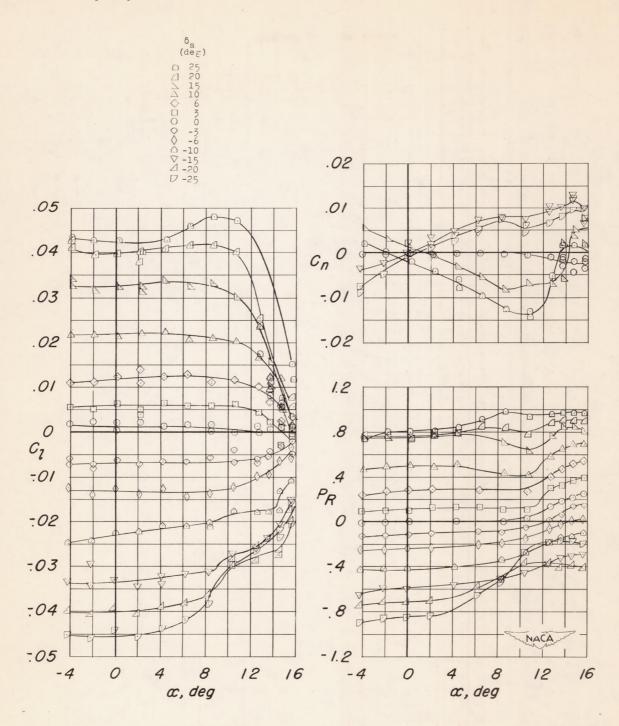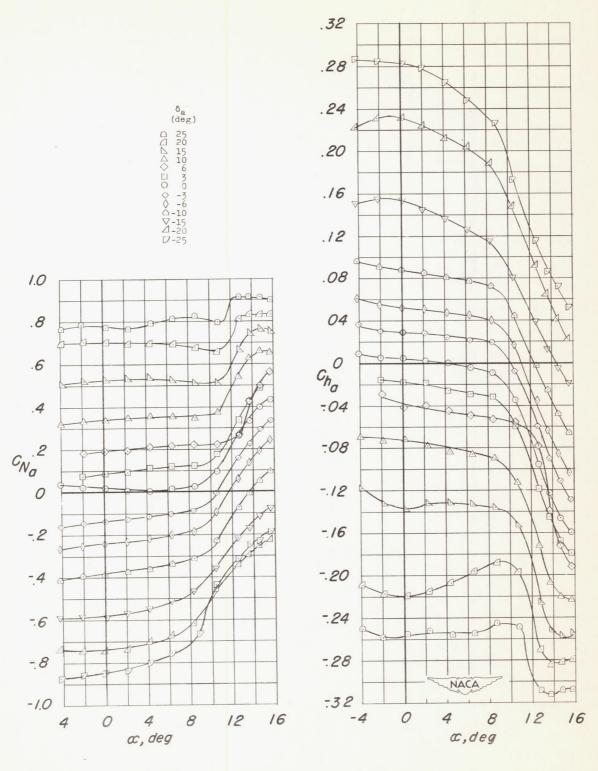
Figure 10.- Variation of P_R, C_{N_a}, C_l, C_n, and C_{h_a} with α; plain wing, 0.75b/2 aileron, t = 0, 0.005c vent, $\delta_f = 0$, $\delta_n = 0$.

(a) Variation of P_R, C_l, and C_n with α.

Figure 11.- Variation of P_R, C_{N_a}, C_l, C_n, and C_{h_a} with α; wing-fuselage combination, 0.75b/2 aileron, t = 0, 0.005c vent, δ_f = 0, δ_n = 0.

(b) Variation of C_{h_a} and C_{N_a} with α.

Figure 11.- Concluded.
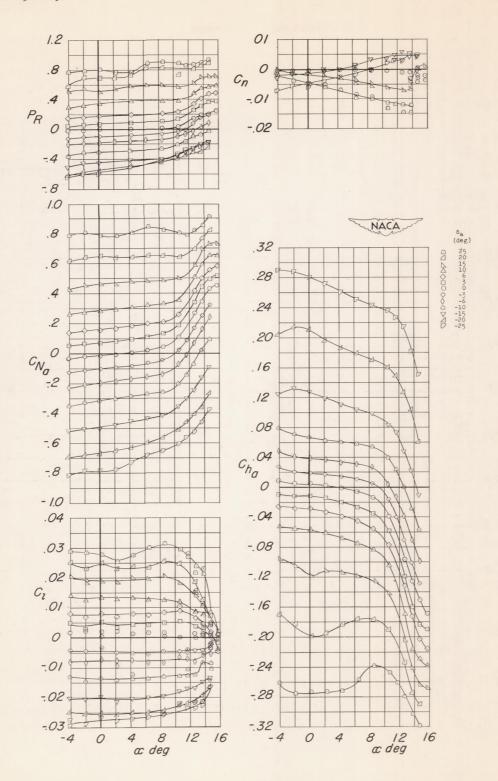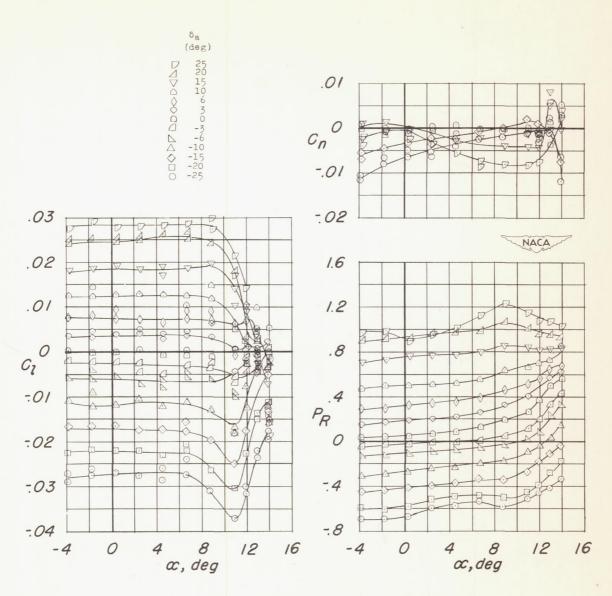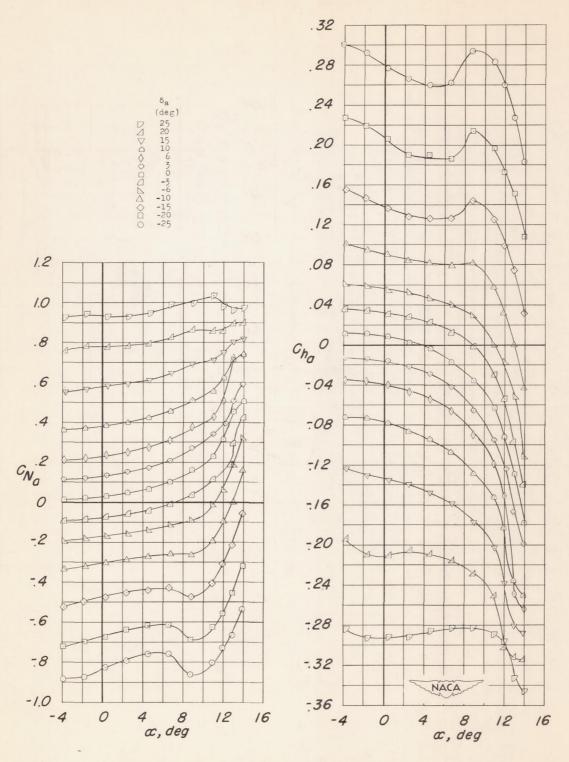
Figure 12.- Variation of P_R, C_{N_a}, C_l, C_n, and C_{h_a} with α; wing-fuselage combination, 0.40b/2 aileron, t = 0, 0.005c vent, $\delta_f = 0$, 0.
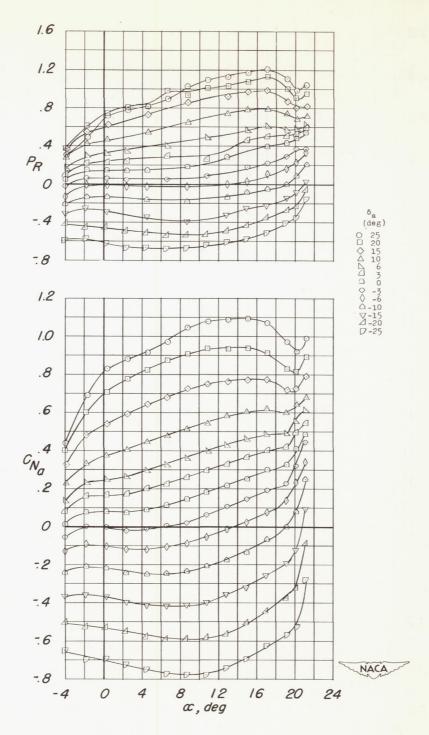
(a) Variation of P_R, C_l, and C_n with α.

Figure 13.- Variation of P_R, C_{N_a}, C_l, C_n, and C_{h_a} with α; wing-fuselage combination, 0.40b/2 aileron, $t = 0$, 0.005c vent, $\delta_f = 50°$ (0.35b flap), $\delta_n = 0$.

(b) Variation of C_{h_a} and C_{N_a} with α.

Figure 13.- Concluded.

δ_a (deg)
○ 25
□ 20
◇ 15
△ 10
◁ 6
◻ 3
◻ 0
◇ -3
◇ -6
△ -10
▽ -15
◁ -20
▽ -25

(a) Variation of P_R and C_{N_a} with α.
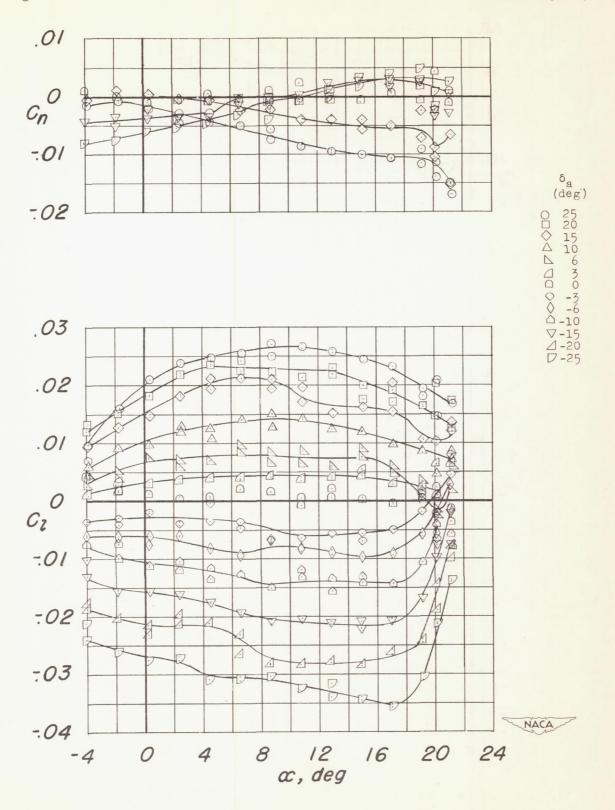
Figure 14.- Variation of P_R, C_{N_a}, C_l, C_n, and C_{h_a} with α; wing-fuselage combination, 0.40b/2 aileron, t = 0, 0.005c vent, $δ_f = 50°$ (0.35b flap), $δ_n = 30°$.
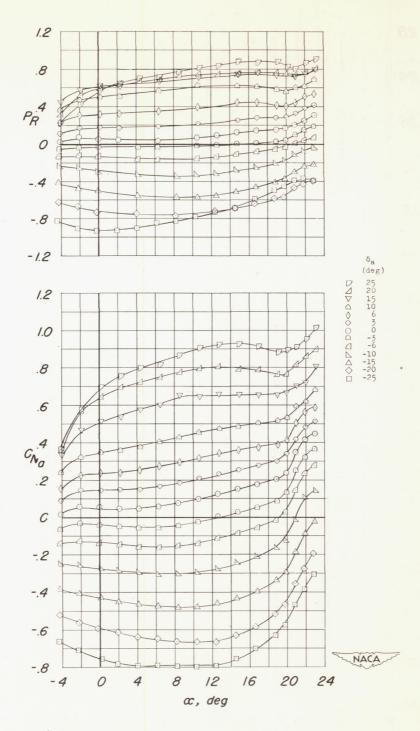
δ_a
(deg)

○ 25
□ 20
◇ 15
△ 10
◁ 6
◺ 3
⬠ 0
◇ -3
◇ -6
△ -10
▽ -15
◁ -20
▽ -25

(b) Variation of C_{h_a} with α.
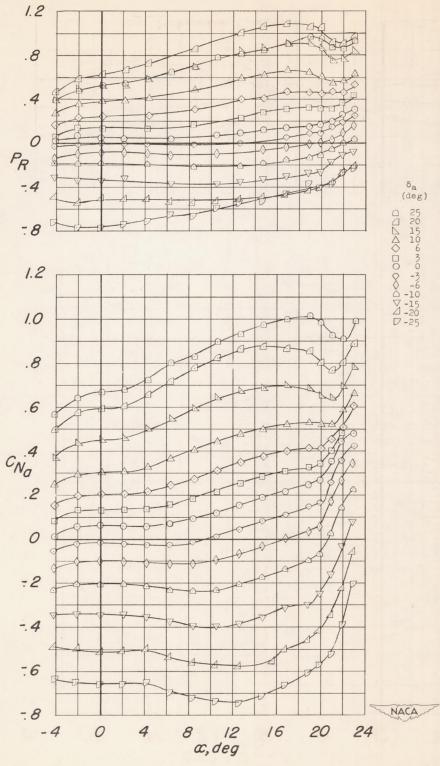
Figure 14.- Continued.
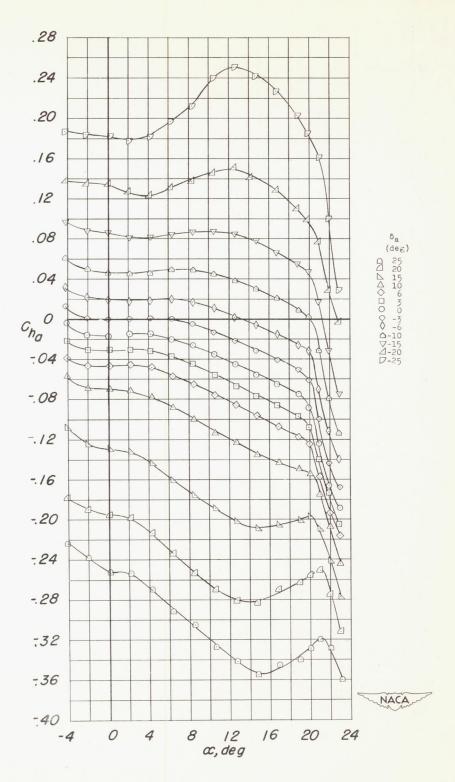
(c) Variation of C_l and C_n with α.

Figure 14.- Concluded.

(a) Variation of P_R and C_{N_a} with α.
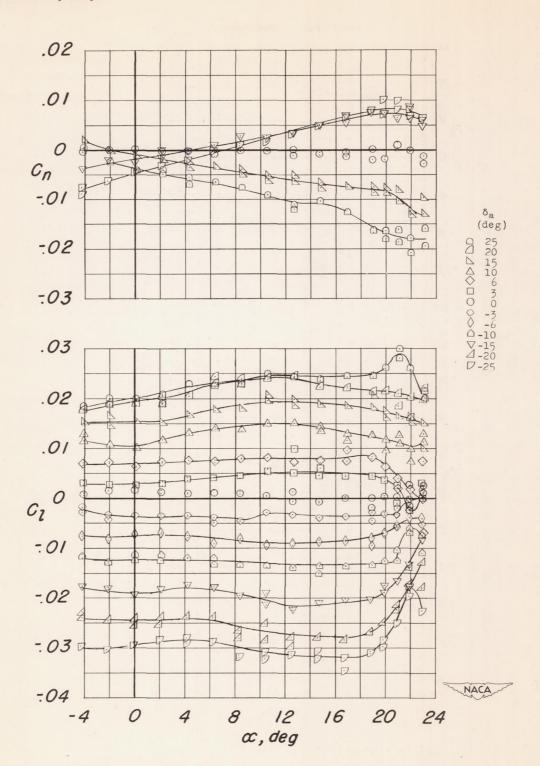
Figure 15.- Variation of P_R, C_{N_a}, C_l, C_n, and C_{h_a} with α; wing-
   fuselage combination, 0.40b/2 aileron, $t = 0$, 0.005c vent, $\delta_f = 0$,
   $\delta_n = 30^o$.

(b) Variation of C_{h_a} with α.

Figure 15.- Continued.
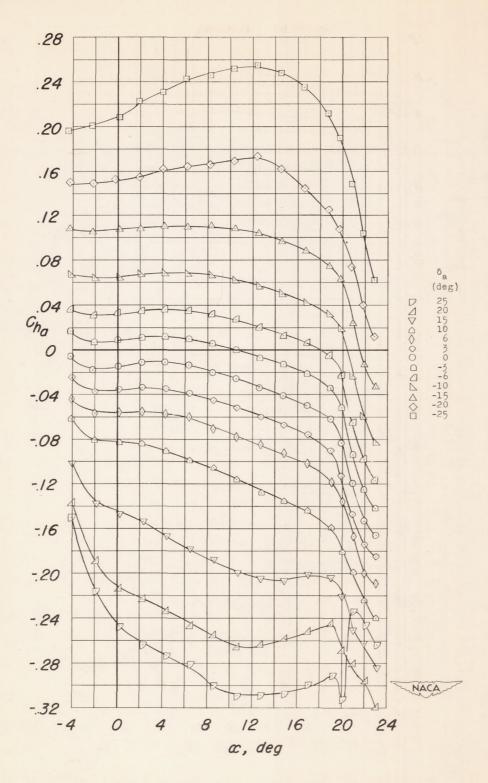
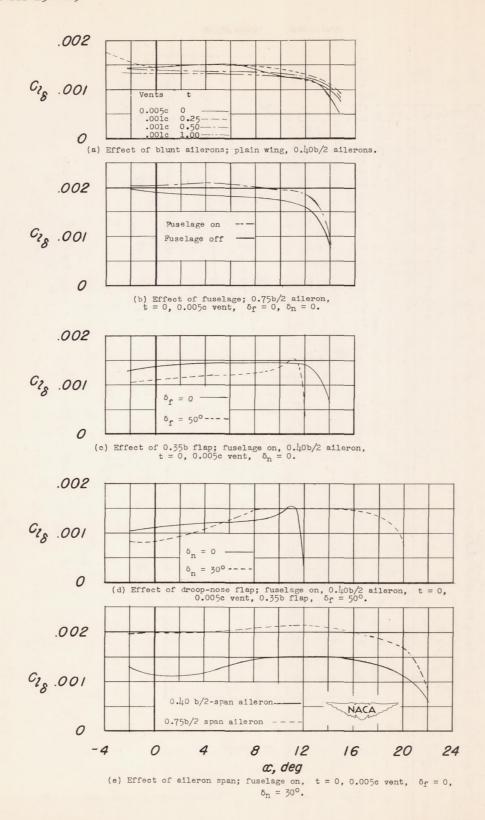(c) Variation of C_l and C_n with α.

Figure 15.- Concluded.

(a) Variation of P_R and C_{N_a} with α.
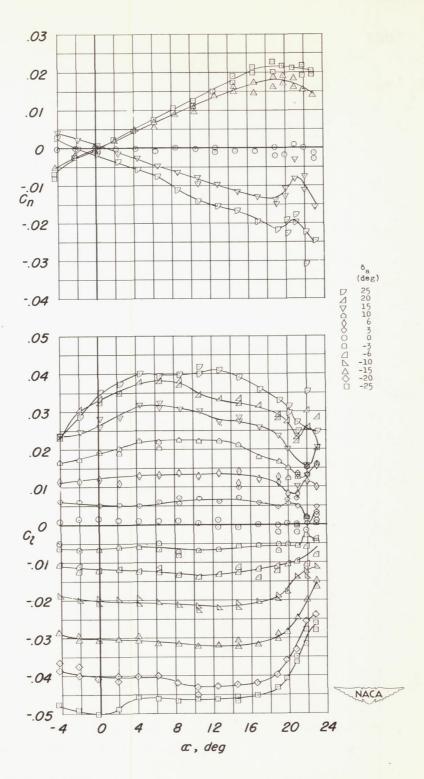
Figure 16.- Variation of P_R, C_{N_a}, C_l, C_n, and C_{h_a} with α; wing-fuselage combination, 0.75b/2 aileron, t = 0, 0.005c vent, δ_f = 0, δ_n = 30°.

(b) Variation of C_{h_a} with α.

Figure 16.- Continued.

(c) Variation of C_l and C_n with α.

Figure 16.- Concluded.

(a) Effect of blunt ailerons; plain wing, 0.40b/2 ailerons.

Vents	t
0.005c	0
.001c	0.25
.001c	0.50
.001c	1.00

(b) Effect of fuselage; 0.75b/2 aileron,
t = 0, 0.005c vent, $\delta_f = 0$, $\delta_n = 0$.

Fuselage on
Fuselage off

(c) Effect of 0.35b flap; fuselage on, 0.40b/2 aileron,
t = 0, 0.005c vent, $\delta_n = 0$.

$\delta_f = 0$
$\delta_f = 50°$

(d) Effect of droop-nose flap; fuselage on, 0.40b/2 aileron, t = 0,
0.005c vent, 0.35b flap, $\delta_f = 50°$.

$\delta_n = 0$
$\delta_n = 30°$

(e) Effect of aileron span; fuselage on, t = 0, 0.005c vent, $\delta_f = 0$,
$\delta_n = 30°$.

0.40 b/2-span aileron
0.75b/2 span aileron

Figure 17.- Effect of various leading-edge and trailing-edge devices on
the aileron effectiveness parameter C_{l_δ}.

O Present investigation
☐ Reference 9
◇ Reference 10
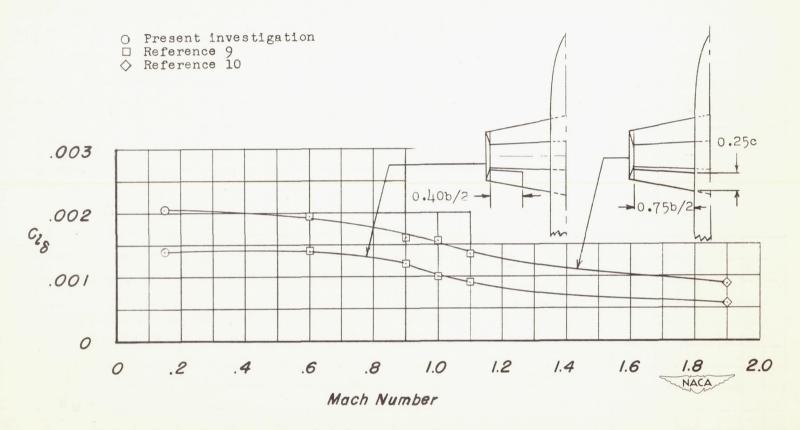
Figure 18.- Variation of aileron effectiveness parameter C_{l_δ} with Mach number. Reynolds number varies from 10^6 to 7.6×10^6.
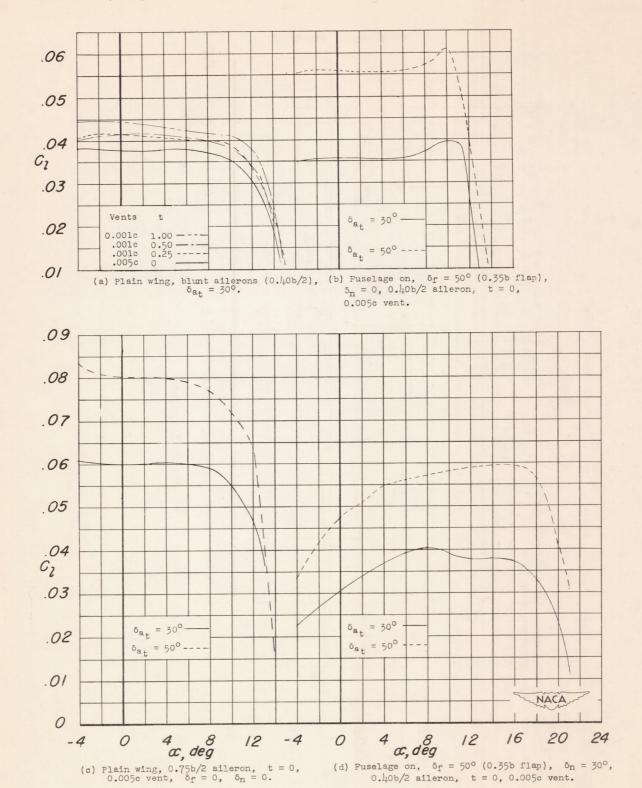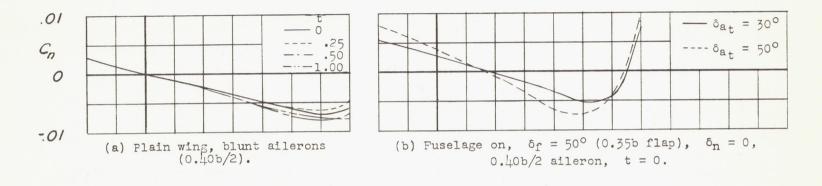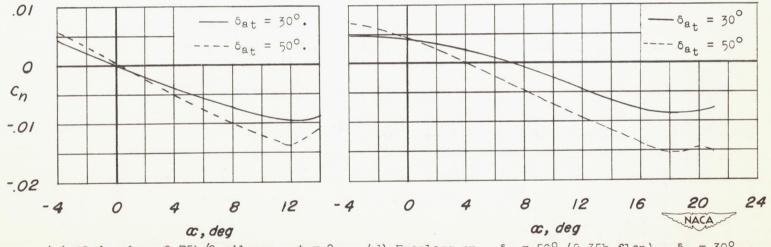
(a) Plain wing, blunt ailerons (0.40b/2), $\delta_{a_t} = 30°$.

(b) Fuselage on, $\delta_f = 50°$ (0.35b flap), $\delta_n = 0$, 0.40b/2 aileron, t = 0, 0.005c vent.

(c) Plain wing, 0.75b/2 aileron, t = 0, 0.005c vent, $\delta_f = 0$, $\delta_n = 0$.

(d) Fuselage on, $\delta_f = 50°$ (0.35b flap), $\delta_n = 30°$, 0.40b/2 aileron, t = 0, 0.005c vent.

Figure 19.- Rolling-moment coefficients for total aileron deflections of 30° and 50°.

Figure 20.- Yawing-moment coefficients for total aileron deflections
of 30° and 50°.

(a) Plain wing, blunt ailerons (0.40b/2).

(b) Fuselage on, $\delta_f = 50°$ (0.35b flap), $\delta_n = 0$, 0.40b/2 aileron, t = 0.

(c) Plain wing, 0.75b/2 aileron, t = 0.

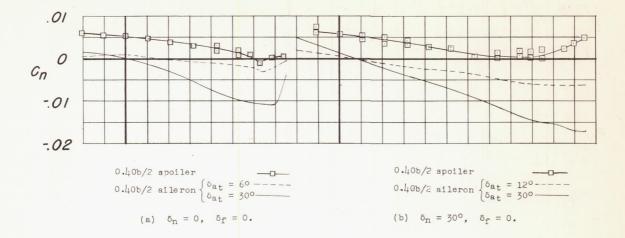(d) Fuselage on, $\delta_f = 50°$ (0.35b flap), $\delta_n = 30°$, 0.40b/2 aileron, t = 0.
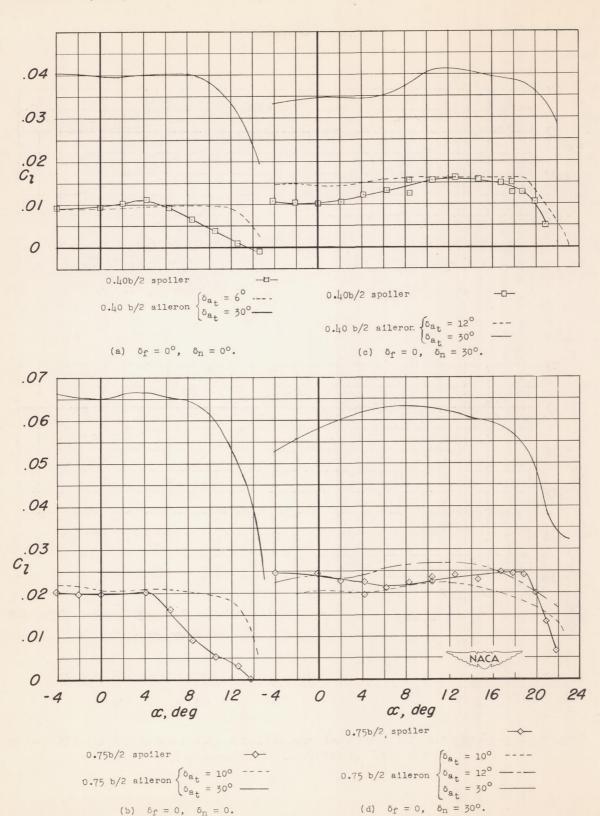
Figure 21.- Comparison of spoiler and aileron rolling-moment coefficients
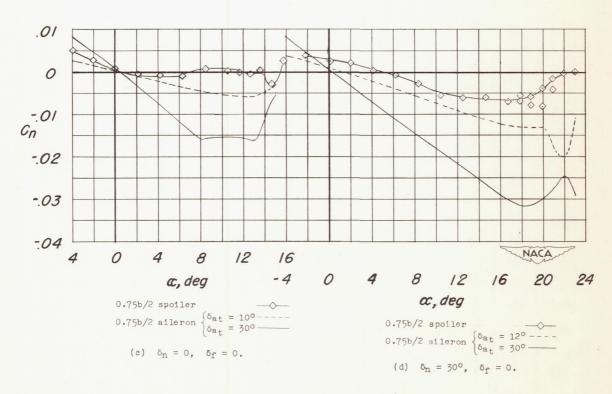for various configurations. Fuselage on, t = 0, 0.005c vent.

Figure 22.- Comparison of spoiler and aileron yawing-moment coefficients
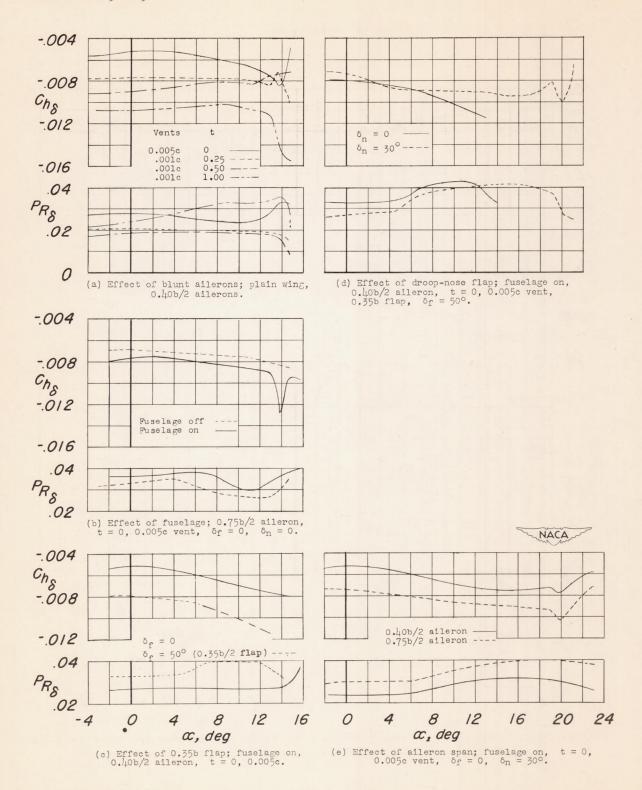for various configurations. Fuselage on, t = 0.

(a) Effect of blunt ailerons; plain wing, 0.40b/2 ailerons.

(b) Effect of fuselage; 0.75b/2 aileron, t = 0, 0.005c vent, δ_f = 0, δ_n = 0.

(c) Effect of 0.35b flap; fuselage on, 0.40b/2 aileron, t = 0, 0.005c.

(d) Effect of droop-nose flap; fuselage on, 0.40b/2 aileron, t = 0, 0.005c vent, 0.35b flap, δ_f = 50°.

(e) Effect of aileron span; fuselage on, t = 0, 0.005c vent, δ_f = 0, δ_n = 30°.

Figure 23.- Aileron deflection hinge-moment parameters and resultant balance-chamber pressure-coefficient parameters for various configurations.
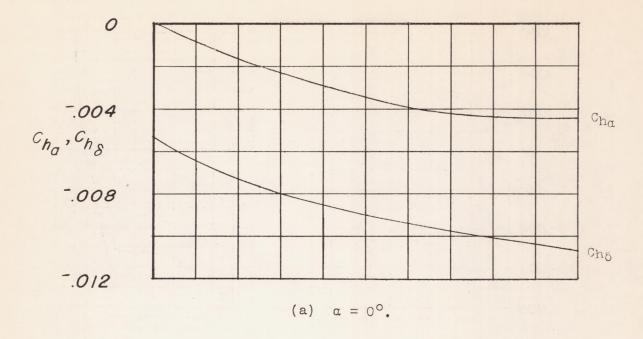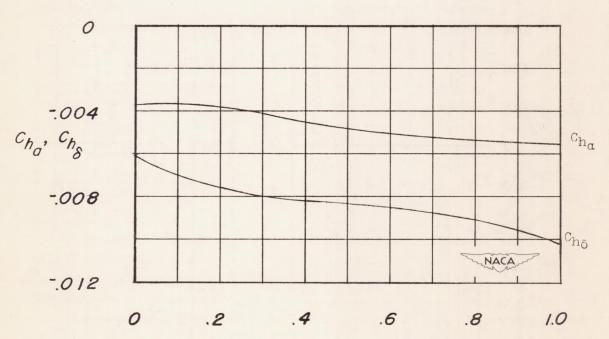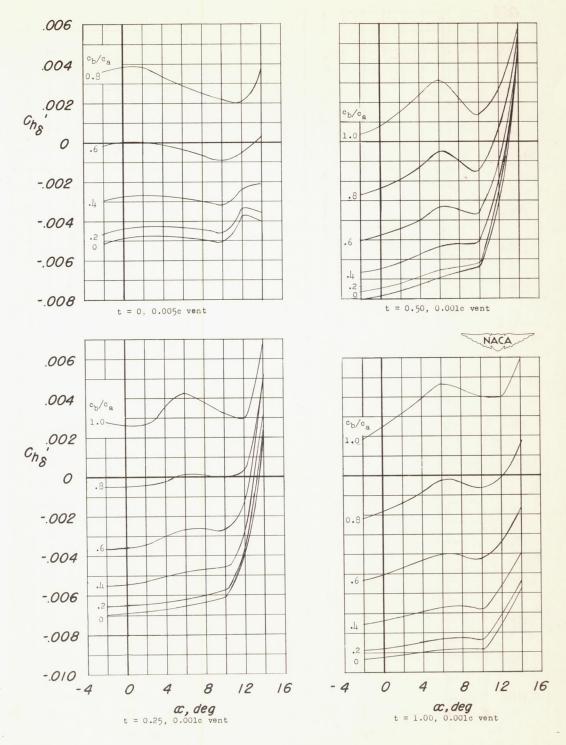
(a) Effect of blunt ailerons;
    plain wing, 0.40b/2 ailerons.

(c) Effect of droop-nose flap; fuselage on,
    0.40b/2 aileron, t = 0, 0.005c vent,
    0.35b flap, δ_f = 0.

(b) Effect of fuselage; 0.75b/2
    aileron, t = 0, 0.005c vent,
    δ_f = 0, δ_n = 0.

(d) Effect of aileron span; fuselage on, t = 0,
    0.005c vent, δ_f = 0, δ_n = 0.
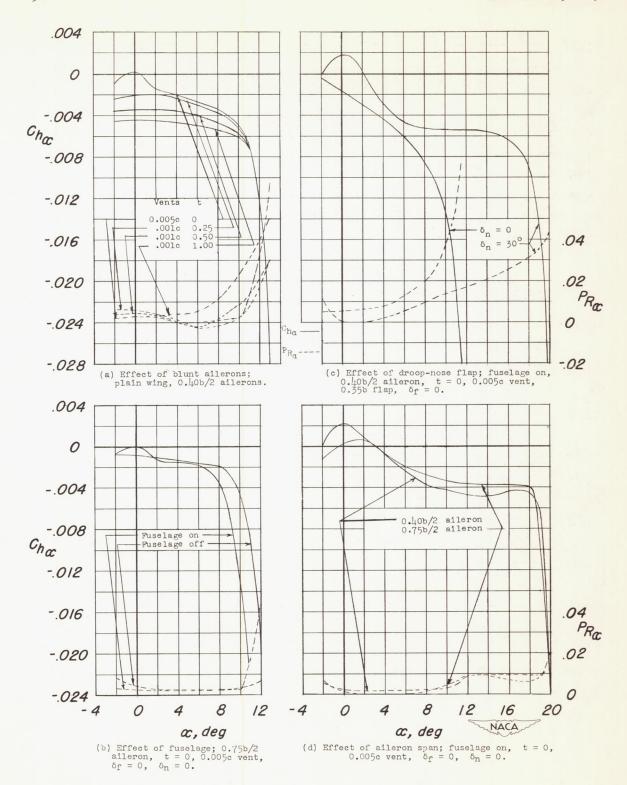
Figure 24.- Aileron angle-of-attack hinge-moment parameters and resultant
    balance-chamber pressure-coefficient parameters for various configurations.
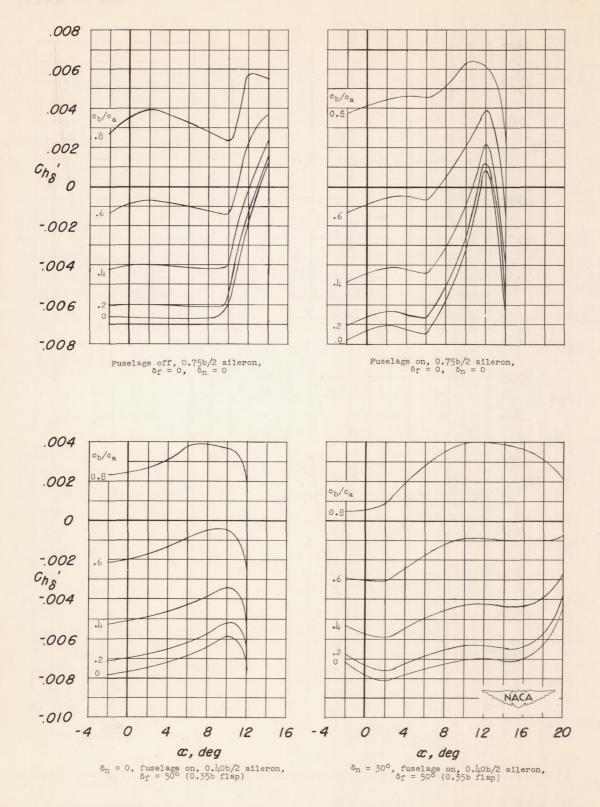
(a) $\alpha = 0°$.

(b) $\alpha = 8.5°$.

Figure 25.- Effect of aileron trailing-edge thickness on aileron hinge-moment parameters. 0.40b/2 aileron, plain wing.

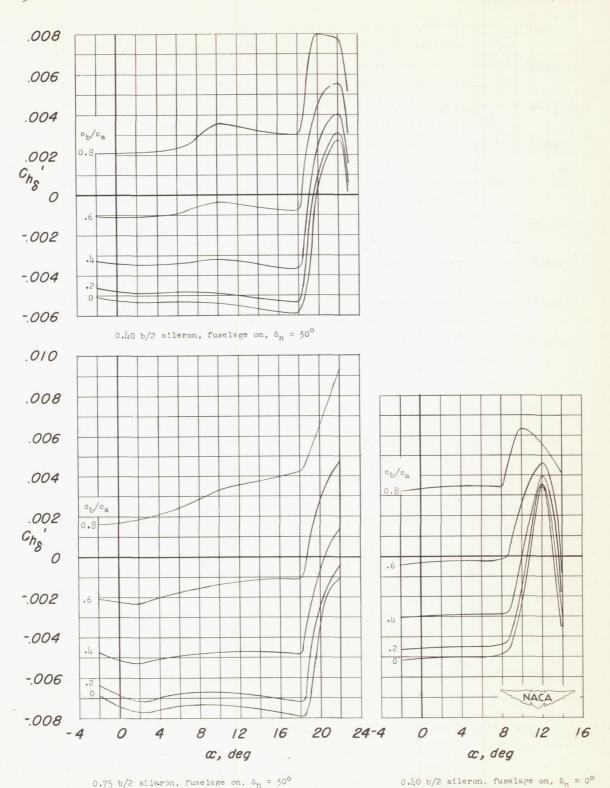(a) Effect of aileron trailing-edge thickness; 0.40b/2 aileron, plain wing.

Figure 26.- Aileron hinge-moment parameter $C_{h_\delta}{}'$ in a steady roll for various balance-chord ratios.
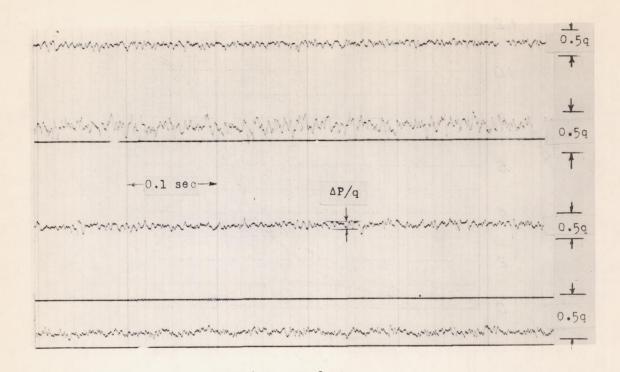
Fuselage off, 0.75b/2 aileron,
$\delta_f = 0$, $\delta_n = 0$

Fuselage on, 0.75b/2 aileron,
$\delta_f = 0$, $\delta_n = 0$

$\delta_n = 0$, fuselage on, 0.40b/2 aileron,
$\delta_f = 50°$ (0.35b flap)

$\delta_n = 30°$, fuselage on, 0.40b/2 aileron,
$\delta_f = 50°$ (0.35b flap)

(b) Effects of a fuselage and droop-nose flap; 0.005c vent.

Figure 26.- Continued.

0.40 b/2 aileron, fuselage on, $\delta_n = 30°$

0.75 b/2 aileron, fuselage on, $\delta_n = 30°$

0.40 b/2 aileron, fuselage on, $\delta_n = 0°$

(c) Effect of aileron span; 0.005c vent, $\delta_f = 0$.

Figure 26.- Concluded.
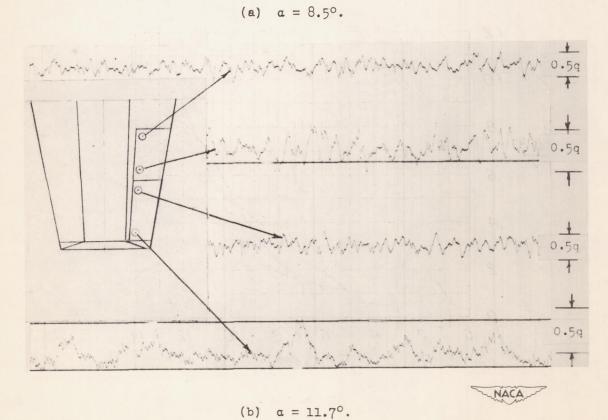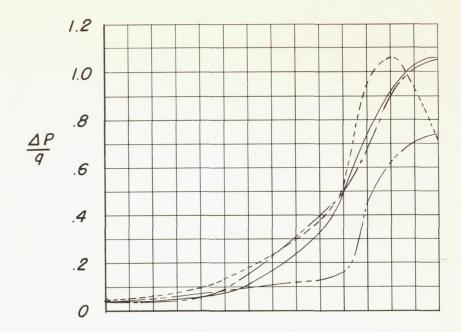
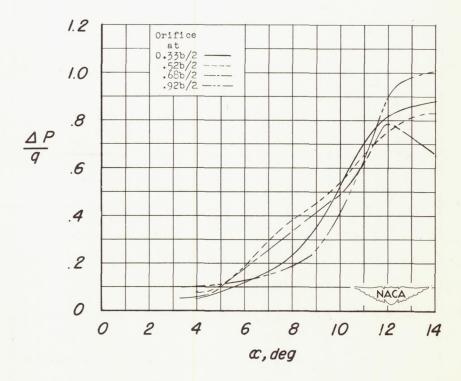(a) α = 8.5°.

(b) α = 11.7°.

Figure 27.- Time history of fluctuating pressure differential between upper
and lower surfaces; plain wing, $\delta_a = 15^\circ$, t = 0, 0.005c vent.

(a) $\delta_a = 4°$.

(b) $\delta_a = 15°$.

Figure 28.- Average fluctuation of pressure at $0.10c_a$ behind aileron hinge-line ($0.40b/2$ aileron deflected); plain wing, $t = 0$, $0.005c$ vent.